fects of irradiation geometry and density-temperature profiles so that the relation between these velocities is well understood. Because peak x-ray emission emanates from the most dense region of the shell, the final values are not greatly different. These calculations also show that the shell is exploded by superthermal electrons to a fuel-pusher interface velocity approaching 10^7 cm/sec, and is then driven by thermal-electron pressure at approximately constant acceleration for the duration of the implosion. Applying this parabolic-trajectory model to the dashed lines of Figs. 1 and 2, one determines acceleration values in the range of $(3.4-4.2)\times10^{17}$ cm/sec^2. The agreement of the measured velocity and acceleration values with the more detailed histories of the respective computations tends to confirm our physical models for energy transport in these exploding pusher target experiments.

In conclusion, we have presented detailed measurements of the spatially and temporally resolved dynamics of laser-imploded fusion targets. These results provide the first direct measures of target implosion velocity and acceleration, and are consistent with theoretical modeling of the exploding-pusher process.

The authors wish to acknowledge the contributions of their colleagues H. G. Ahlstrom, J. H. Nuckolls, J. E. Swain, R. F. Wuerker, B. W. Weinstein, C. H. Dittmore, and J. W. Houghton.

*Work performed under the auspices of the U. S. Energy Research and Development Administration.

[1]J. Nuckolls, L. Wood, A. Thiessen, and G. Zimmerman, Nature (London) 239, 139 (1972).

[2]P. M. Cambell, G. Charatis, and G. R. Monty, Phys. Rev. Lett. 34, 74 (1975).

[3]F. Seward, J. Dent, M. Boyle, L. Koppel, T. Harper, P. Stoering, and A. Toor, Rev. Sci. Instrum. 47, 464 (1976).

[4]V. W. Slivinsky, H. G. Ahlstrom, K. G. Tirsell, J. Larsen, S. Glaros, G. Zimmerman, and H. Shay, Phys. Rev. Lett. 35, 1083 (1975).

[5]D. T. Attwood, L. W. Coleman, J. T. Larsen, and E. K. Storm, Phys. Rev. Lett. 37, 499 (1976); references to similar instruments cited therein.

[6]J. F. Holzrichter and D. R. Speck, J. Appl. Phys. 47, 2459 (1976).

[7]J. E. Swain, H. G. Ahlstrom, A. Glass, K. R. Manes, E. K. Storm, F. Rienecker, J. A. Monjes, D. E. Campbell, and L. Seppala, Bull. Am. Phys. Soc. 21, 1029 (1976), and to be published.

[8]D. T. Attwood, B. W. Weinstein, and R. F. Wuerker, "Composite X-Ray Pinholes for Time-Resolved Microphotography of Laser Compressed Targets" (to be published).

[9]The 6-μm-diam pinhole, as described in Ref. 8, is laser-drilled in a 60%-Ta_2O_5 silicate glass, which is subject to damage from the unabsorbed laser light and from general target debris.

[10]Time-integrated x-ray microphotographs for these targets do not display the familiar ring pattern (Refs. 2 and 3) associated with targets of larger radius and lower absorbed power per unit mass.

[11]J. T. Larsen, Bull. Am. Phys. Soc. 21, 1029 (1976).

Motion of Clusters on Surfaces

Uzi Landman, Elliott W. Montroll, and Michael F. Shlesinger*
Institute for Fundamental Studies, Department of Physics and Astronomy, University of Rochester, Rochester, New York 14627
(Received 5 November 1976)

A stochastic model of the diffusion of atomic clusters on crystalline surfaces, capable of treating complex systems, has been developed. Novel methods allow the analysis of diffusion data in field-free and -biased experiments. Expressions for the complete determination of parameters characterizing the individual cluster configurations from measurable quantities are derived.

The observation of the motion of atomic species on surfaces with resolution power of atomic dimensions became available only recently,[1-6] mainly through the use of field-ion-microscopy[7] (FIM) techniques. An important observation is that adatoms can form small clusters which diffuse (as exhibited on several fcc and bcc metal surfaces[2-6,8-12]) by undergoing transitions between the possible cluster configurations. The nature of the motion depends on the surface morphology [e.g., one-dimensional (1D) "channeled" diffusion of tungsten clusters on the (211) plane of W (Refs. 8–10) versus 2D diffusion of platinum clusters on the (110) plane of W (Refs. 5, 11, and 12)]. Also, under the influence of high electric fields, directional migration of clusters can be effected.[5,13]

Of basic importance in the construction and evaluation of theories of processes like thin-film

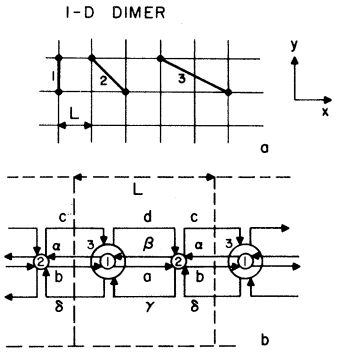

FIG. 1. 1D dimer migration. (a) Three possible spatial configurations of a dimer (filled circles connected by heavy line) moving along the x direction (the allowed equivalent mirror image configurations are not included in the figure). If only states 1 and 2 are allowed, a two-state dimer; if all states are allowed, a three-state dimer. (b) The random-walk lattice describing the motion of the dimer centroid in (a). The unit cell is denoted by dashed lines and the states by circles, numbered respectively. Lettered arrows indicate transitions to and from states. Note that transition rates connecting states can be different for transitions to the left or right (i.e., $a \neq \alpha$). Also the centroid location is the same for states 1 and 3; however, they are distinguished by different transition rates.

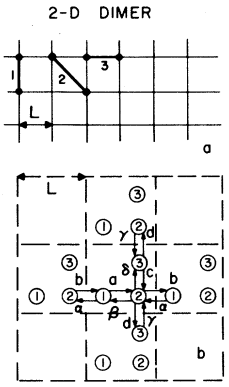

FIG. 2. 2D dimer migration. (a) Spatial configurations; (b) random-walk lattice.

and crystal growth,[14] sintering,[15] and surface reactions[16] is the ability *to deduce* elementary physical quantities which control the motion of atoms and aggregates on surfaces (such as activation energies, frequency factors, and interatomic potentials) and to understand the effects due to structure and morphology on the displacement mechanisms and rates.[1,17] We present here the principles of a theory, employing stochastic techniques, which allows the determination of physical parameters which characterize the motion of arbitrarily complex clusters for variable kinetics and dimensionality. Previous analysis[18] could not treat the common case where the cluster has the same center of mass for different configurations, and was also limited to one dimension and did not include a bias field. Except for the case of a dimer with two internal states,[19] FIM data were analyzed by calculating the ill-defined quantity of "an average transition rate" for the cluster rather than the individual rates between the cluster configurations.[2-12] We show that to calculate the individual rates, *full use must be made* of the FIM data, which consist of measurements of diffusion distances and probabilities of occurrence of different configurations as a function of temperature. Furthermore, we show that the application of a bias is necessary for the complete determination of the individual rates for certain clusters (e.g., a dimer with three states in one dimension; see below).

Model.—A cluster of atoms on a surface can exist in several spatial configurations between which transitions occur. The location of the *centroid* of the cluster[18] can be *mapped* onto a periodic lattice on which it performs a random walk. The unit cell of the random-walk lattice will contain, generally, several "*sites*," or *internal states*. To illustrate the above, consider the following examples: (1) the motion in one dimension of a dimer which can exist in three distinct states (configurations) (see Fig. 1), and (2) the motion of a dimer in two dimensions (see Fig. 2).

In Figs. 1(a) and 2(a) the allowed dimer configurations (in coordinate space) are shown. The centroid location of the dimers undergoes a random walk on the lattices shown in Figs. 1(b) and 2(b) (unit cells are denoted by dashed lines and their internal states by numbered circles). We note that the centroid can have the same spatial location for distinctly different spatial configurations (for example, states 1 and 3 in Fig. 1). The transition rates between the allowed states are given in Figs. 1(b) and 2(b) by the lettered arrows. In addition, allowing for $a \neq \alpha$, $b \neq \beta$, etc., a directional preference (bias) to the motion is introduced.

We calculate the motion of the cluster using the formalism of continuous-time random walk[20] (CTRW) with internal states[21] (as we discuss elsewhere,[21] this description is equivalent to a generalized master equation with internal states). Let us introduce the waiting-time distribution matrix $\underline{\psi}(\vec{l}, t)$ whose elements govern the individ-

ual transitions. The element $\psi_{ij}(\vec{l}, t)dt$ is the probability density that a transition between the internal states $j \to i$, in unit cells separated by $\vec{l}$, occurs in the time interval $(t, t+dt)$. Since all the observables can be represented in terms of $\underline{\psi}$, we explicitly exhibit it, for the case shown in Fig. 1:

$$\underline{\psi}(\vec{l}, t) = \begin{bmatrix} 0 & e^{-Ut}(b\delta_{L,-1}+\beta\delta_{L,0}) & 0 \\ e^{-At}(a\delta_{L,0}+\alpha\delta_{L,-1}) & 0 & e^{-Dt}[d\delta_{L,0}+(\delta)\delta_{L,-1}] \\ 0 & e^{-Ut}(c\delta_{L,1}+\gamma\delta_{L,0}) & 0 \end{bmatrix}, \quad (1)$$

where $A=a+\alpha$, etc., and $U=B+C$. In the following we will employ the following form for activated-process transition rates:

$$\left.\begin{matrix} a \\ \alpha \end{matrix}\right\} = \nu_a \exp\{-[E_a \pm g(V)]/kT\}, \quad (2)$$

etc., where ν_a is the frequency factor, T is the absolute temperature, and E_a and V are the activation energy and bias voltage, respectively.[22] By use of discrete Fourier (with respect to the lattice) and Laplace (with respect to the continuous time variable) transforms, the convolution theorems, and Green's-function techniques, the semi-Markov chain relation for the random walk can be solved. This yields expressions[21,23] for the moments of the probability distribution, $P_{ji}(\vec{l}, t)$, for the centroid to reach the jth internal state in the $\vec{l}$th unit cell at a time t if initially it was in the zeroth (origin) cell with probability p_i of being in state i. Calculating the first moment

$$\langle \vec{l}(t) \rangle = \sum_{i,j,\vec{l}} \vec{l} P_{ji}(\vec{l}, t) p_i,$$

and its variance, we find in the long-time limit for the 1D three-state dimer (case 1)

$$t^{-1}\langle l_3(t) \rangle = Z^{-1}[A(cd-\gamma\delta)+D(ab-\alpha\beta)], \quad (3)$$

$$t^{-1}\sigma_3^2(t) = Z^{-1}[A(cd+\gamma\delta)+D(ab+\alpha\beta)] + 6Z^{-1}\langle l_3(t)\rangle^2 t^{-2}(A+B+C+D), \quad (4)$$

where $Z=AC+BD+AD$. In the absence of bias and excluding the most extended state (state 3, Fig. 1) of the dimer (i.e., $c \to 0$, $d \to \infty$), $\langle l_3(t) \rangle$ vanishes and $\sigma_3^2(t)$ reduces to $t^{-1}ab(a+b)^{-1}$, previously obtained by Reed and Ehrlich[18] (the factor-of-4 difference between the result in Ref. 18 and the present one is due to unit-cell definitions).

The relationship between the variances of the three-state and two-state 1D dimers (σ_3^2 and σ_2^2, respectively), in the absence of a bias field and when the transition rates characterizing the latter (a, b) remain the same upon the introduction of the third state (Fig. 1), is shown in Fig. 3.

Since the forces holding the atomic cluster together involve long-ranged dispersion forces, it is expected that extended configurations, such as the one shown in Fig. 1(a) (state 3), can occur. As shown above, their inclusion in the model can affect significantly the predictions for the observables and the values for E and ν derived from them. Consequently, FIM data should be examined for such occurrences. It should be emphasized that these and more general possibilities (for example, motion in two dimensions, discussed below), cannot be treated by previous methods,[18] since the latter cannot include states for which the centroid of the cluster coincide.

Methods of analysis.—One of the objectives in developing the model outlined above is to make possible the extraction of parameters [E and ν, Eq. (2)] which characterize the states of the system under study. As the simplest example, consider the biased 1D motion of a two-state dimer (shown in Fig. 1 with state 3 forbidden). The ratio, $R_{12}(T)=ab^{-1}$, of the probabilities of occupation of states 1 and 2 can be determined (detailed balance) from the random-walk formalism and

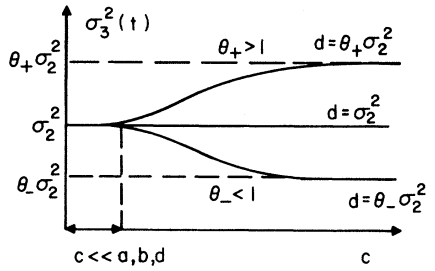

FIG. 3. Behavior of the variance, $\sigma_3^2(t)$, of the field-free three-state dimer (Fig. 1) as a function of transition rate c $(2 \to 3)$, when all the parameters characterizing the two-state dimer remain unchanged. Note differences in behavior for different choices of the return transition rate d $(3 \to 2)$. When the transition rate d from the extended state 3 to state 2 equals the variance of the two-state dimer, $\sigma_3^2(t)$ equals $\sigma_2^2(t)$ regardless of the values of the other transition rates.

empirically. Utilizing this relation yields

$$a = t^{-1}\langle l_2(t)\rangle f(V, T)[1 + R_{12}(T)], \quad (5)$$

for the transition rate a [Eq. (2)], where

$$f(V, T) = 2^{-1}\,\mathrm{csch}[g(V)/kT]\,\exp[-g(V)/kT]. \quad (6)$$

A semilog plot of the right-hand side of Eq. (5), with experimental values for $\langle l_2(t)\rangle$ and $R_{12}(T)$, as a function of $(kT)^{-1}$ yields a straight line of slope E_a and intercept ν_a. Replacing $R_{12}(T)$ by its inverse yields the equation for b. Similarly, expressions for a and b can be derived in terms of $R_{12}(T)$, $\sigma_2^2(t)$, and functions of V and T. However, we suggest the use of Eq. (5) since here the statistical error involved in the determination of the mean location is smaller than in the determination of the variance.[24]

In bias-free experiments the mean vanishes and the data consist of the variance and the relative population of states as functions of the temperature. In this case a is given by[19]

$$a = t^{-1}\sigma_2^2(t)[1 + R_{12}(T)], \quad (7)$$

and similarly for b with R_{12} replaced by its inverse. A plot of the logarithm of the rhs of (7) versus $(kT)^{-1}$ allows the determination of E_a and ν_a (and similarly E_b and ν_b) as the slope and intercept, respectively, of the resulting straight lines. Clearly, by adopting the standard practice[2-13] of plotting $\ln\sigma^2$ against $(kT)^{-1}$, a determination of E_a and ν_a (and E_b, ν_b) cannot be made since the cluster diffusion *cannot be described by a single Arrhenius relationship* [see Eqs. (3) and (4)]. Note that although the latter semilog plot would appear to be almost a straight line in the typical temperature range of the experiments, its slope and intercept *are not simply related* to the quantities characterizing the individual states.

The discussion of the 1D motion of a three-state dimer involves four transition rates [Fig. 1(b)]. Thus we need four independent relationships. Detailed balance between the three dimer states provides us with two relationships and the variance gives a third one. To determine the transition rates fully in this case, an external field *must* be applied and the mean $\langle l_3(t)\rangle$ be measured. As shown above, for a two-state dimer this is not necessary, although preferable.

For the 2D motion of a two-state dimer (Fig. 2) several alternatives for the extraction of the characteristic transition rates can be exercised dictated by the type of experiment performed (depending mainly on whether a bias field is applied or not). For example, in the case of a bias-free measurement, our analysis yields the transition rates in terms of the observed (as a function of temperature) variances (σ_x^2, σ_y^2) and the state occupation ratios (R_{12} and R_{23}; see Fig. 2):

$$b = \sigma_x^2(1 + R_{12} + R_{23}^{-1})t^{-1}, \quad (8a)$$

$$a = bR_{12}^{-1}, \quad c = b\sigma_y^2/\sigma_x^2, \quad d = cR_{23}. \quad (8b)$$

Semilogarithmic plots of the above four relations, using measured quantities from FIM micrographs, versus $(kT)^{-1}$ allow the determination of the individual frequency factors and activation energies.

The above theoretical study demonstrates that by employing the *full* information content of FIM data (including bias-field experiments which are necessary for some systems, as discussed above) in proper methods of analysis, a complete determination of transition rates of diffusing clusters on surfaces can be made. Moreover, this analysis allows the characterization of elementary microscopic steps of the motion of clusters on surfaces which would enable detailed studies of migration mechanisms, interaction potentials, and the substrate-geometry dependency of cluster motion on metal surfaces. Finally the formalism presented here could be reduced to a computational algorithm which would allow us to analyze the dynamics of complex clusters on surfaces. Effects due to defects and boundary conditions other than the periodic ones used above can be easily incorporated.[24] The theory provides a framework for the formulation and analysis of a stochastic theory of film growth and reaction kinetics on surfaces.

---

*Xerox Research Fellow.

[1]G. Ehrlich, CRC Crit. Rev. Solid State Sci. 4, 205 (1974).

[2]G. Ehrlich and F. G. Hudda, J. Chem. Phys. 44, 1039 (1966).

[3]D. W. Bassett and M. T. Parsley, J. Phys. D 3, 707 (1970).

[4]W. R. Graham and G. Ehrlich, Thin Solid Films 25, 85 (1975).

[5]T. T. Tsong, P. Cowan, and G. Kellog, Thin Solid Films 25, 97 (1975).

[6]D. W. Bassett and D. R. Tice, in *The Physical Basis of Heterogeneous Calalysis*, edited by E. Dragulis and R. J. Jaffee (Plenum, New York, 1975).

[7]E. W. Müller and T. T. Tsong, *Field Ion Microscopy* (Elsevier, New York, 1969).

[8]W. R. Graham and G. Ehrlich, Phys. Rev. Lett. 31, 1407 (1973).

[9]W. R. Graham and G. Ehrlich, J. Phys. F 4, 2212 (1974).
[10]D. A. Reed and G. Ehrlich, Philos. Mag. 32, 1095 (1975).
[11]D. W. Bassett, in *Surface and Defect Properties of Solids*, edited by M. W. Roberts and J. M. Thomas (Chemical Society, London, 1973), Vol. 2, p. 34.
[12]D. W. Bassett, J. Phys. C 4, 2491 (1976).
[13]T. T. Tsong and R. J. Walko, Phys. Status Solidi (a) 12, 111 (1972).
[14]D. Elwell and H. J. Scheel, *Crystal Growth from High Temperature Solutions* (Academic, New York, 1975).
[15]J. M. Blakely, Prog. Mater. Sci. 10, 395 (1963); G. E. Rhead, Scr. Metallogr. 6, 47 (1972).
[16]G. Ertl and J. Küppers, *Low Energy Electrons and Surface Chemistry* (Verlag Chemi, Weinheim, 1974).
[17]H. P. Bonzel, CRC Crit. Rev. Solid State Sci. 6, 171 (1976); G. E. Rhead, Surf. Sci. 47, 207 (1975).
[18]D. A. Reed and G. Ehrlich, J. Chem. Phys. 64, 4616 (1976).
[19]Since the completion of this work, a study of the 1D motion of Re dimers of W(211) has been published, in which a proper analysis is given; see Stolt, W. R. Graham, and G. Ehrlich, J. Chem. Phys. 65, 3206 (1976).
[20]E. W. Montroll and G. Weiss, J. Math. Phys. (N.Y.) 6, 167 (1965); H. Scher and M. Lax, Phys. Rev. B 7, 4491 (1973); E. W. Montroll and H. Scher, J. Stat. Phys. 9, 101 (1973); M. F. Shlesinger, *ibid.*, 10, 421 (1974).
[21]U. Landman, E. W. Montroll, and M. F. Shlesinger, Proc. Nat. Acad. Sci., U. S. A. (February, 1977). For a discussion of random walk with internal states, see also E. W. Montroll, J. Math. Phys. (N.Y.) 10, 753 (1969).
[22]The function $g(V)$ describes the bias-field dependence of the activation energy [see Ref. 13 and S. Nisigaki and S. Nakamura, Jpn. J. Appl. Phys. 15, 1647 (1976)].
[23]U. Landman, E. W. Montroll, and M. F. Shlesinger, to be published.
[24]From a comparison of results obtained from the analysis of biased and bias-free data, the effect of external fields on the transition rates could be investigated.

Self-Consistent Approximation to the Hubbard Model*

E. N. Economou and C. T. White†
Department of Physics, University of Virginia, Charlottesville, Virginia 22901
(Received 20 October 1975; revised manuscript received 27 December 1976)

The Hubbard model is studied by employing a random-potential approximation, which incorporates the effects of magnetic ordering and dynamical processes. Comparison of our results to existing data on one-dimensional systems shows that the present approximation is very accurate over the whole range of values of the physical parameters.

Hubbard,[1] in his treatment of the Hamiltonian

$$\hat{\mathcal{H}} = \sum_{i\sigma} \epsilon_0 \hat{n}_{i\sigma} + \sum_{ij\sigma} V_{ij} \hat{a}_{i\sigma}^{\dagger} \hat{a}_{j\sigma} + U \sum_i \hat{n}_{i\uparrow} \hat{n}_{i\downarrow}, \quad (1)$$

replaced the last term by a one-body random potential

$$U \hat{n}_{i\uparrow} \hat{n}_{i\downarrow} \approx \epsilon_{i\sigma} \hat{n}_{i\sigma}, \quad (2)$$

where $\epsilon_{i\sigma}$ was taken as U or 0 with equal probability. In Eq. (1), the sites $\{i\}$ form a lattice, σ takes two values [down ($\downarrow$) or up ($\uparrow$)], ϵ_0 is a constant, V_{ij} is usually taken (for simplicity) as a constant V when i and j are nearest neighbors and zero otherwise, $\hat{a}_{i\sigma}^{\dagger}$ and $\hat{a}_{i\sigma}$ are creation and annihilation operators of a local state at the site i with spin σ, and $\hat{n}_{i\sigma} = \hat{a}_{i\sigma}^{\dagger} \hat{a}_{i\sigma}$. Subsequently,[2] $\epsilon_{i\sigma}$ was taken as $\frac{1}{2}U(1+\tilde{\mu})$ or $\frac{1}{2}U(1-\tilde{\mu})$, where $\tilde{\mu}$ was obtained self-consistently and was interpreted as the size of a local moment, the z component of which can take on two values, $\pm\tilde{\mu}$. This approach to the problem, though an improvement over the original Hubbard treatment, misses two important features of the model: (1) The influence of the magnetic ordering (MO) on the electronic properties is omitted except for the limiting cases of perfect order or no order at all; thus, this effect is treated satisfactorily only at the extreme temperatures, $T=0$ or $T=\infty$. (ii) The dynamic processes (DP), which allow μ_{iz} to change with time from $+\tilde{\mu}$ to $-\tilde{\mu}$ and vice versa, are neglected; the local moments are "frozen" in a particular configuration.

In the formalism summarized below, MO (equivalent to an Ising coupling) is incorporated in a self-consistent way, and its effect on the electronic structure is included. Furthermore, it is argued that DP amount to replacing the Ising by a Heisenberg coupling. With the present incorporation of MO and DP, one can provide strong evidence that a satisfactory understanding of the behavior of the Hubbard model has been achieved.